Photoinduced Disorder in Strongly Segregated Block Copolymer Composite Films for Hierarchical Pattern Formation

Li Yao and James J. Watkins*

Department of Polymer Science and Engineering, University of Massachusetts Amherst, 120 Governors Drive, Amherst, Massachusetts 01003, United States

ABSTRACT Submicrometer patterns of adjacent, well-ordered and disordered domains were obtained using optical lithography by area-selective, photoinduced disordering transitions within block copolymer composite films. Enantiopure tartaric acid was blended with poly(ethylene oxide-block-*tert*-butyl acrylate), PEO-*b*-PtBA, copolymers to yield well-ordered films. In the presence of triphenylsulfonium triflate, a photoacid generator, photoinduced disorder was achieved upon UV-exposure by deprotection of the PtBA block to yield poly(acrylic acid). Poly(acrylic acid) is compatible with both PEO and tartaric acid and deprotection yields a phase mixed material and disorder within seconds. Tartaric acid performs two additional functions in this system. First, it increases segregation strength in PEO-*b*-PtBA, enabling well-ordered systems at low BCP molecular weights, small domain sizes, and rapid disordering kinetics. Second, the presence of tartaric acid suppresses PEO crystallization, resulting in smooth films and eliminating the influence of PEO crystallization on film morphology.

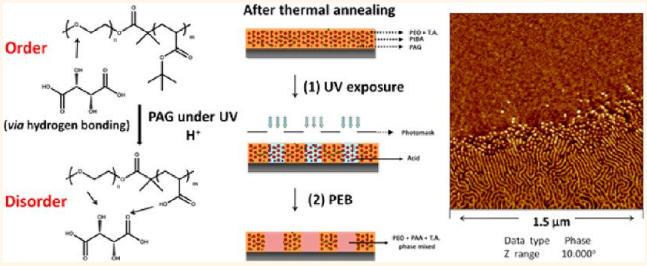

KEYWORDS: block copolymer · phase separation · enantiopure tartaric acid additive · photoinduced disordering transition · hierarchical pattern formation

Block copolymer (BCP) self-assembly has emerged in recent years as a very attractive method for the fabrication of functional nanostructured materials[1−4] and also for the development of next-generation lithography[5−8] for the semiconductor industry. By tuning the number of repeat units (N), the segment−segment interaction parameter, known as the Flory−Huggins parameter (χ), and volume fraction (f) of each segment, BCPs can be designed such that they self-assemble into well-ordered periodic morphologies with domain sizes typically on the order of 5−30 nm.[9] Long range order and preferred orientations of the domains can further be realized through the use of solvent vapor annealing,[10−16] external fields,[17−20] directed self-assembly,[21−31] and/or interfacial interactions.[32−36] Additives can also be used to increase the segregation strength. For example,[37,38] the addition of a homopolymer that can selectively interact with one of the block copolymer segments can significantly enhance segregation strength. Furthermore, small functional molecules[39,40] or nanoparticles[41] that can interact preferentially with one of the blocks, can induce order in otherwise disordered BCPs, producing composite materials that have applications in a variety of areas including electronics,[21] photovoltaics,[42−44] and photonics.[45,46]

Recently, much effort has been directed toward achieving light-induced ordering or disordering transitions in block copolymer systems.[47,48] Such approaches would yield readily accessible pathways toward hierarchical structures in which nanoscale features are defined *via* block copolymer phase segregation, and device level structures are defined by optical lithography. The most common approaches used to date have been based on photoinduced isomerization of azobenzene[47,49−51] or anthracene[48,52−54] moieties contained within a BCP chain segment. This approach relies on relatively small changes in the apparent segregation strength of the system upon isomerization and thus requires careful tuning of molecular weight

* Address correspondence to watkins@polysci.umass.edu.

Received for review November 14, 2012 and accepted January 10, 2013.

Published online January 10, 2013
10.1021/nn3052956

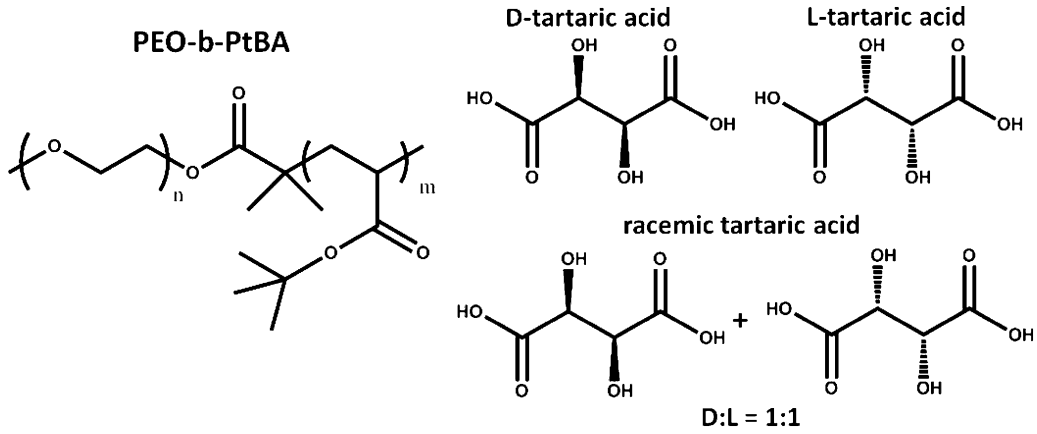

Figure 1. Structures of PEO-*b*-PtBA, D-tartaric acid, L-tartaric acid, and racemic tartaric acid.

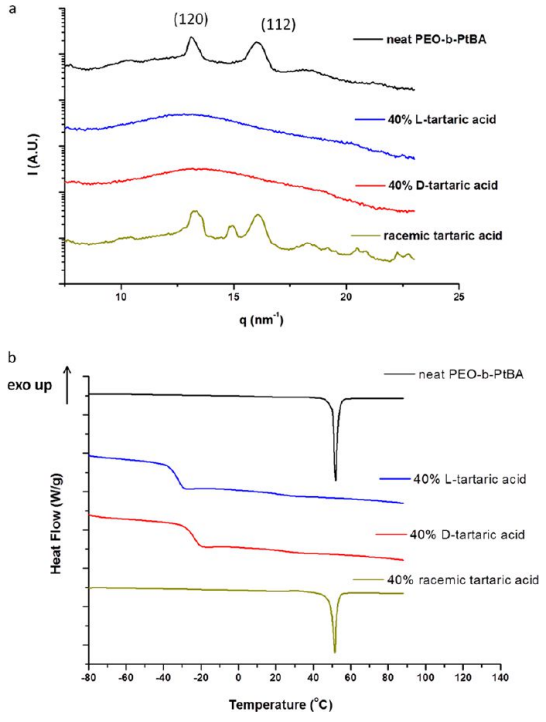

Figure 2. (a) WAXS characterization for neat PEO-*b*-PtBA (9.2K, 46.6 wt % PtBA, PDI = 1.04), PEO-*b*-PtBA blended with 40 wt % L-tartaric acid, 40 wt % D-tartaric acid, and 40 wt % racemic tartaric acid; (b) DSC characterization of neat PEO-*b*-PtBA (9.2K, 46.6 wt % PtBA, PDI = 1.04), PEO-*b*-PtBA blended with 40 wt % L-tartaric acid, 40 wt % D-tartaric acid, and 40 wt % racemic tartaric acid by heating from −90 to 110 °C with a rate of 10 °C/min.

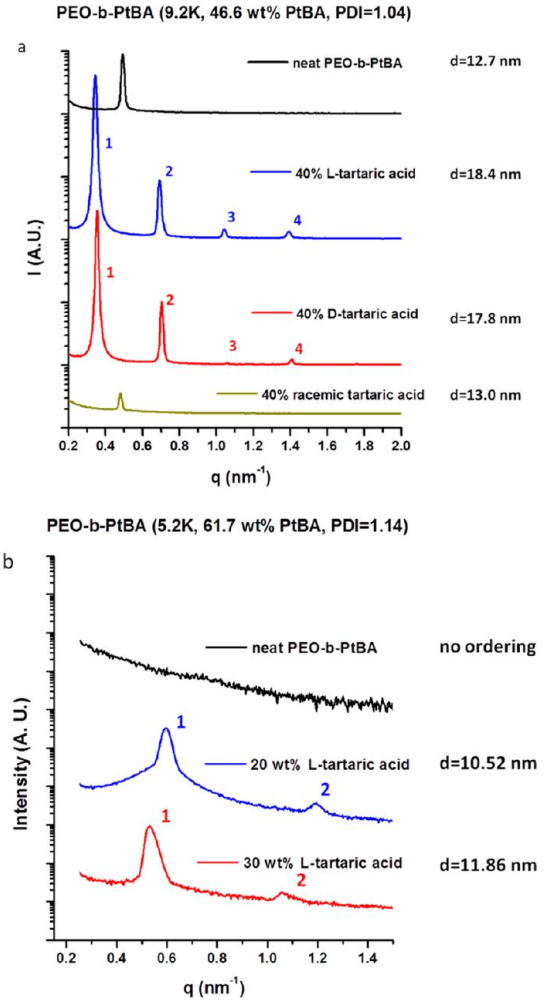

Figure 3. (a) SAXS of neat PEO-*b*-PtBA (9.2K, 46.6 wt % PtBA), PEO-*b*-PtBA with 40 wt % D-tartaric acid, 40 wt % L-tartaric acid, and 40 wt % racemic tartaric acid; (b) SAXS spectra and integrations of PEO-*b*-PtBA (5.2K, 61.7 wt % PtBA, PDI = 1.14) blended with 0 wt % L-tartaric acid, 20 wt % L-tartaric acid, and 30 wt % L-tartaric acid. All samples were annealed at 90 °C for 36 h before tests, and all SAXS data were taken at 90 °C above the melting point of PEO.

such that the critical segregation strength for phase separation can be achieved upon light exposure. Since this will occur over a rather narrow range of molecular weight and because the small changes in the interactions produce limited changes in segregation strength, the versatility of the technique in terms of available domain sizes and the degree of order is somewhat limited.

Recently we described an alternative path to achieve photoinduced order that was based on inducing strong interactions between an additive and one segment of a BCP by chemically amplified deprotection of the additive using a photoacid generator.[55] In that work we

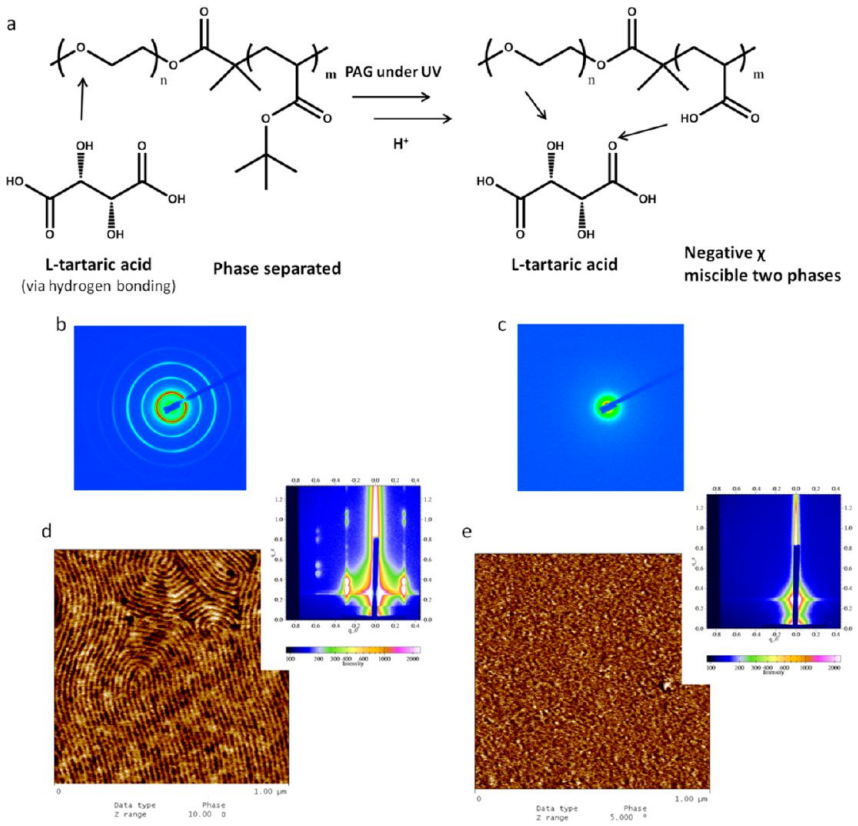

Figure 4. (a) Schematic showing deprotection of PEO-*b*-PtBA (13.9K, 64 wt % PtBA, PDI = 1.12) into PEO-*b*-PAA catalyzed by acid generated from TPS-Tf upon UV flood exposure; (b) SAXS characterization of a bulk sample of PEO-*b*-PtBA blended with 25 wt % L-tartaric acid and 5 wt % TPS-Tf after annealing at 90 °C for 36 h; (c) SAXS characterization of a bulk sample in panel b after UV (254 nm) exposure for 60 s and annealing at 90 °C overnight; (d) AFM characterization and GISAXS spectra of PEO-*b*-PtBA films blended with 25 wt % L-tartaric acid and 5 wt % of TPS-Tf, with a thickness of ∼50 nm after thermal annealing at 90 °C overnight; (e) AFM characterization and GISAXS spectrum of the ordered film in panel d after UV (254 nm) exposure for 60 s and annealing at 90 °C overnight.

used poly(ethylene oxide)-block-poly(propylene oxide)-block-poly(ethylene oxide), PEO-*b*-PPO-*b*-PEO triblock copolymers blended with a protected molecular glass bearing *t*-butyl groups at its periphery and the photoacid generator triphenylsulfonium triflate. Upon light exposure the protected molecular glass was deprotected to remove the *t*-butyl functionality and expose carboxylic acid functionality. These acid groups interact with PEO through a hydrogen bond and drive microphase separation in the exposed regions. While a photoinduced transition from a disordered system to one that exhibited strong segregation was readily achieved, some of the details of this particular system are not conductive to high resolution lithography. First, while PEO crystallization is suppressed in the ordered domains due to the strong interaction with the deprotected additive, it crystallizes in the disordered domains in the absence of the hydrogen bond interaction. Consequently in thin films there is a disparity in surface roughness between the smooth ordered domains and the disordered domains containing PEO crystallites. Second the low glass transition temperatures of the PEO and PPO components contribute to facile acid diffusion, which works against high resolution lithography.

In this report we describe an alternative system that enables high resolution lithography to yield patterned regions of strongly segregated and disordered domains. Instead of using the aforementioned disorder-to-order approach, here we use a photoinduced order-to-disorder scheme to achieve submicrometer scale patterns of ordered and disordered domains. The initially ordered system comprises a poly(ethylene oxide-block-*tert*-butyl acrylate), PEO-*b*-PtBA, blended with tartaric acid. The interaction between the tartaric acid not only inhibits the crystallization of PEO, but also effectively enhances the phase segregation strength of PEO-*b*-PtBA. The increase in segregation strength in the presence of the additive has obvious advantages including the ability to achieve order in low molecular weight systems. The PtBA block can be deprotected in the presence of a photoacid generator to form poly(acrylic acid) (PAA). PAA is compatible with both PEO and tartaric acid and thus deprotection results in a phase mixed material. Using a mask and photoacid generator, area selective photoinduced disorder can be realized upon UV exposure, followed by a postexposure bake (PEB). We further show that through a kinetic study and process optimization for this process, it takes only seconds to complete the disordering transition

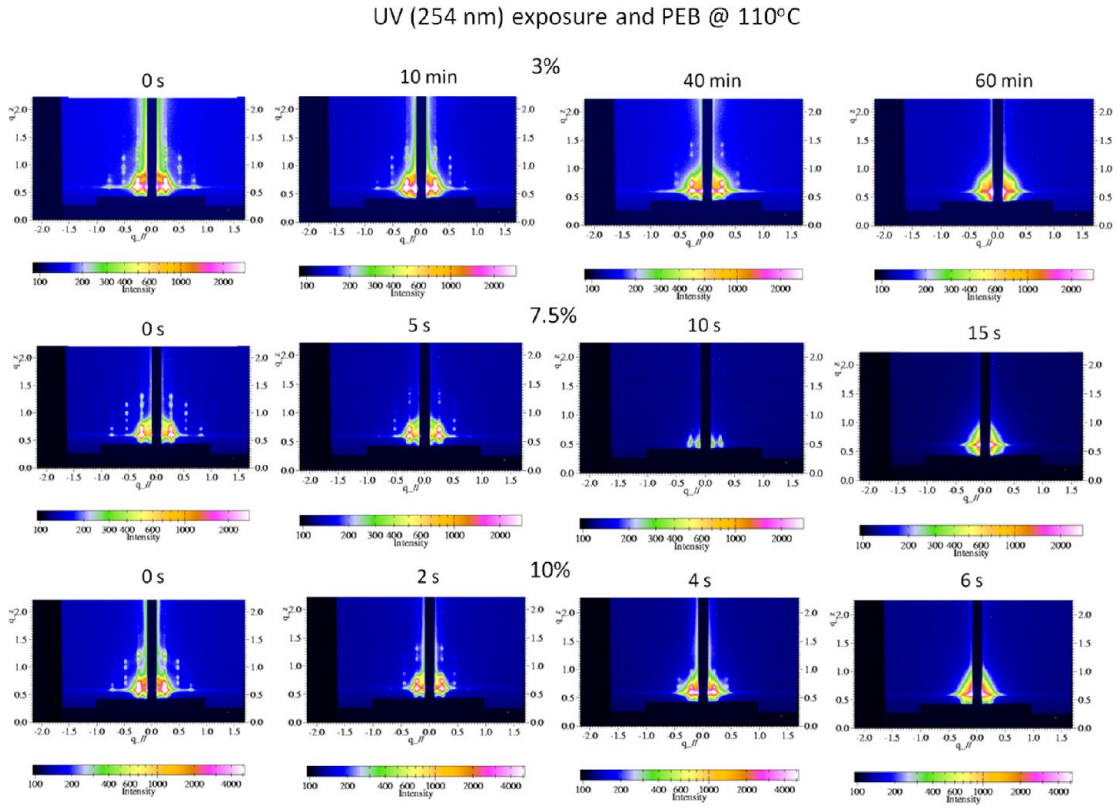

Figure 5. Kinetic study of the order−disorder transition during PEB at 110 °C using GISAXS after UV (254 nm) exposure for 60 s. Three different amounts of TPS-Tf were added to PEO-*b*-PtBA (18K, 72.3 wt % PtBA, PDI = 1.12) blended with 22 wt % L-tartaric acid: 3 wt %, 7.5 wt %, and 10 wt %.

during the PEB, which minimizes acid diffusion. Upon the addition of a trace amount of base to improve resolution, a standard approach in optical lithography, we show that submicrometer patterns of ordered and disordered region structures can be achieved.

RESULTS AND DISCUSSION

Phase-Separation of Block Copolymers Driven by an Enantiopure Tartaric Acid Additive. Tartaric acid is a chiral acid with two stereocenters in its backbone that contains two carboxylic acids and two hydroxyl groups as shown in Figure 1. Enantiomerically pure D- and L-tartaric acid as well as racemic tartaric acid were investigated as additives in this study. The block copolymer was poly(ethylene oxide-*b*-*tert*-butyl acrylate) (PEO-*b*-PtBA). The initial studies were conducted using a BCP of Mn 9.2K, 46.6 wt % PtBA, PDI = 1.04, which in the neat melt is weakly segregated. Both this copolymer and another copolymer of lower molecular weight (5.2K), which is disordered in the melt, were used to probe the phase behavior of the BCP/tartaric acid systems. Upon blending enantiopure tartaric acid into the BCPs, the carboxylic acid and hydroxyl group of the tartaric acid can strongly interact with the PEO block through hydrogen bonding. The effect of the interaction of the PEO block with the additive on the crystallization behavior of PEO was investigated using wide-angle X-ray scattering (WAXS) and differential scanning calorimetry (DSC). WAXS results (Figure 2a) show peaks at 13.2 and 16.2 nm^{-1}, which correspond to (120) and (112) planes in the PEO unit cell, respectively, indicating the presence of PEO crystallites for neat BCP samples, while no crystal peaks were present with the addition of enantiopure tartaric acid, indicating the strong interaction between PEO and enantiopure acid. This interaction inhibits crystallization of both PEO and tartaric acid. However, when racemic tartaric acid was added to the system, peaks indicating crystallization of both PEO and tartaric acid were observed as shown in Figure 2a, indicating little interaction between them. (WAXS characterizations of racemic and L-tartaric acid are shown in Figure S1 for reference). The DSC measurements as shown in Figure 2b are consistent with the conclusions of the WAXS study. No melting endotherm for PEO is observed upon the addition of D- or L-tartaric acid, but strong melting endotherms are evident for PEO upon the addition of racemic tartaric acid. The glass transition temperature of PEO is reported to be −64 °C.[56] The glass transition temperatures of the PEO tartaric acid blends are clear in the DSC analysis and range between −20 and −30 °C. The glass transition of PtBA is reported to be 43 °C.[57] Our DSC analysis indicates that T_g values for the low molecular weight PtBA segments in this block copolymer (9.2K, 46.6 wt % PtBA, PDI = 1.04) are approximately 30 °C. (see Figure S2 in Supporting Information.)

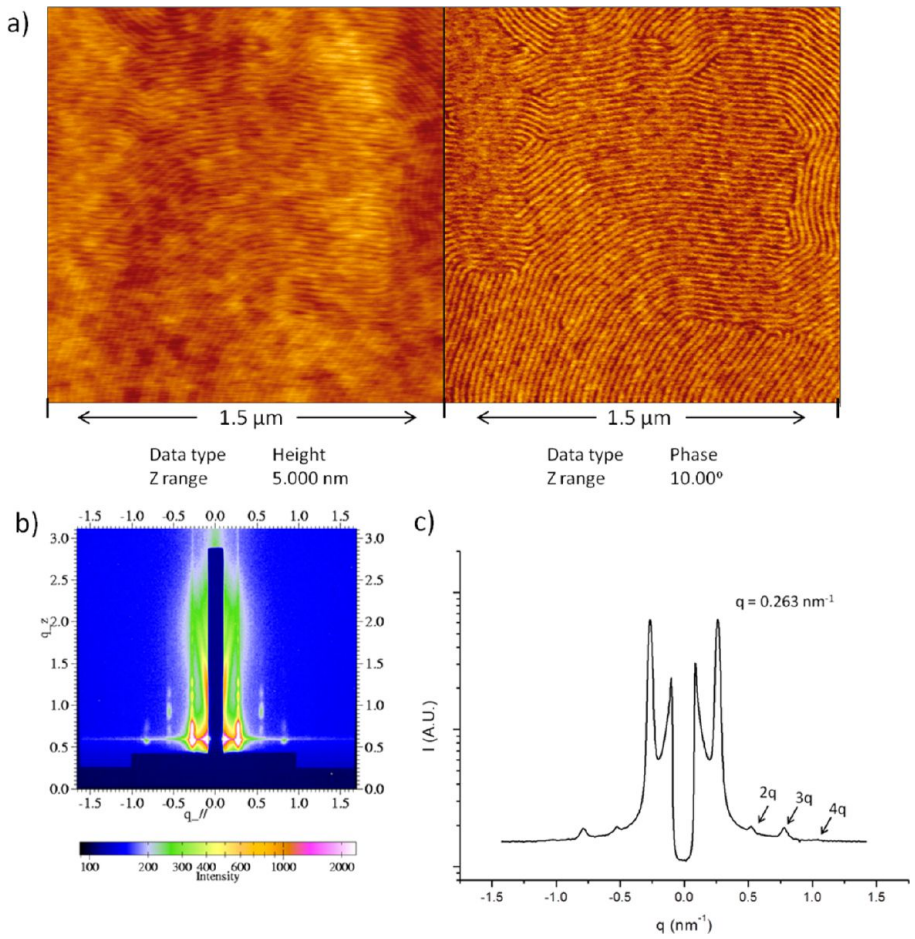

Figure 6. AFM characterization (a) of PEO-*b*-PtBA (18K, 72.3 wt % PtBA, PDI = 1.12) film blended with 22 wt % L-tartaric acid, 10 wt % TPS-Tf, and 0.5 wt % triethanol amine after thermal annealing at 90 °C overnight; GISAXS spectrum (b) and integration (c) for the ordered film in panel a.

As we reported previously,[37,38] the addition of a homopolymer that selectively associates through hydrogen bonding with one segment of low molar mass amphiphilic triblock copolymers can dramatically increase the segregation strength. Small molecule additives can be also effective for increasing segregation strength in block copolymer composites.[40,58−62] Likewise here the enantiopure tartaric acids not only suppress the crystallization of PEO, but also substantially increase the segregation strength of PEO-*b*-PtBA. Figure 3 shows small-angle X-ray scattering (SAXS) analysis for PEO-*b*-PtBA of two different compositions with and without the addition of tartaric acid. Figure 3a indicates that neat BCP with a molecular weight of 9.2K is weakly ordered at 90 °C and exhibits only a primary scattering peak. With the addition of enantiopure, either D- or L-, tartaric acid into this system, the segregation strength was increased and ordering was dramatically improved as evidenced by the significant increasing of the primary peak intensity and the appearance of multiple higher order reflections which can be assigned as lamellar morphologies. The *d*-spacing was also increased with the addition of enantiopure tartaric acid as shown in Figure 3a. In contrast, the addition of racemic tartaric acid in this system did not enhance microphase separation or order in the system. This is consistent with the DSC and WAXS analysis, which suggests that interaction between the racemates is preferred to interaction of either of the racemates with PEO. Phase pair identity density functional theory simulations were used by the Pearl group to identify a racemic heteropair structure which has the lowest energy level for the racemic tartaric acid pair.[63] Thus, there is little interaction between tartaric acid and the PEO segment when equal amounts of D- or L-tartaric acids are present in the system. Figure 3b shows SAXS results for a sample of PEO-*b*-PtBA of low molecular weight (5.2K) with and without the addition of L-tartaric acid acquired at 90 °C. While the neat copolymer is disordered, the addition of 20% L-tartaric acid is sufficient to induce strong microphase separation, showing lamellar morphology based on a higher order peak in SAXS (Figure 3b). *d*-Spacing was increased by increasing the amount of L-tartaric acid loading, as evidenced by a *d*-spacing of 10.5 nm with 20% L-tartaric acid whereas it was 11.9 nm with 30% L-tartaric acid calculated from SAXS (Figure 3b).

Photoinduced Disorder in Phase-Separated PEO-*b*-PtBA/Tartaric Acid System. Chemically amplified deprotection of

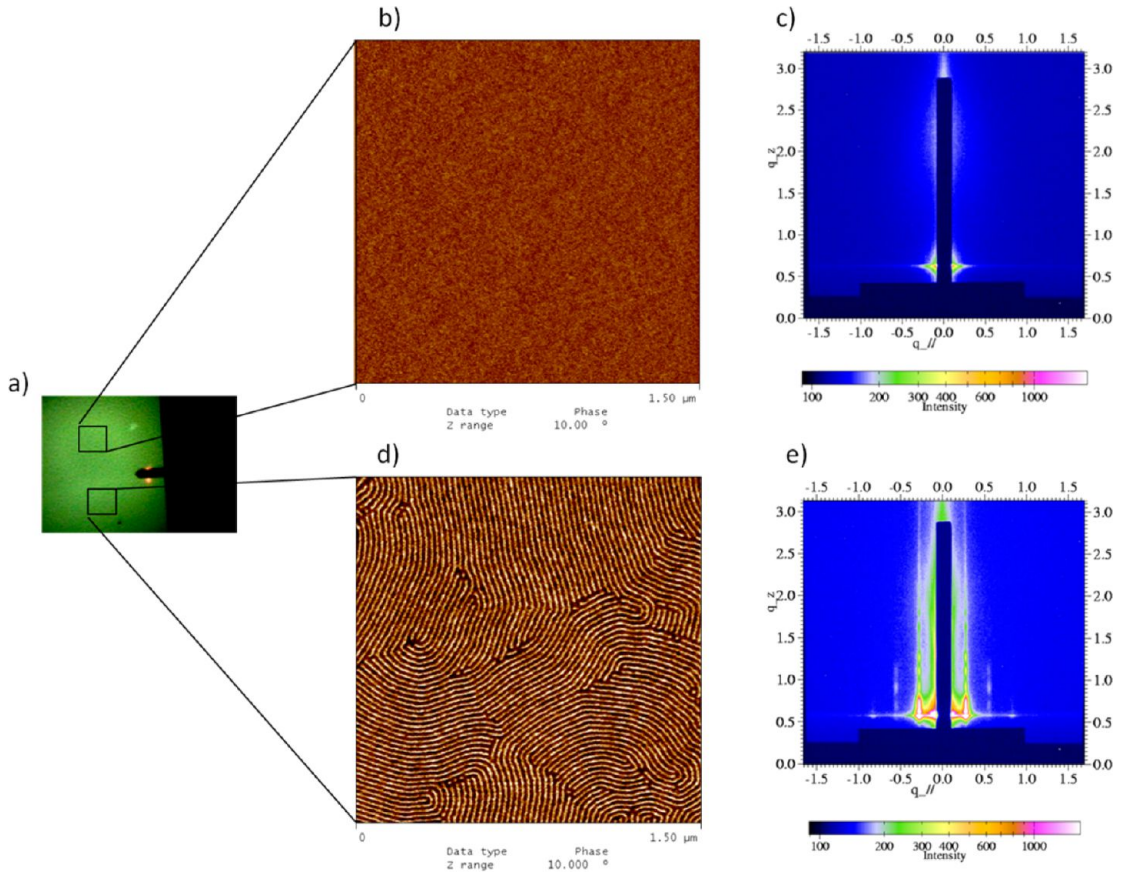

Figure 7. (a) Optical micrograph of the film from Figure 6 after area-selective UV (254 nm) exposure for 60 s using a photomask and a PEB at 110 °C for 10 s showing two regions with a boundary; (b) the UV-exposed region at the top showed disordered structure, as characterized by AFM; (c) the GISAXS spectrum for the film from Figure 6 after UV (254 nm) flood exposure for 60 s and PEB at 110 °C for 10 s; (d) the unexposed region kept its ordered structure, as characterized by AFM; (e) GISAXS spectrum for the film from Figure 6 after baking at 110 °C for 10 s without UV exposure.

resists using photoacid generators for photolithography has been well investigated by many research groups.[64−66] Here we use catalytic deprotection of PtBA induced by the UV exposure of a photoacid generator (PAG) followed by a quick postexposure bake (PEB) to alter the interaction among the resist components and induce disorder. Figure 4 shows the scheme for the photoacid catalyzed, chemically amplified deprotection of the PtBA block to generate PAA at elevated temperatures. PAA interacts strongly with PEO through hydrogen bonding, resulting in a negative χ. The deprotection to PAA generates two miscible blocks each of which is compatible with tartaric acid to form a completely disordered film, as shown in Figure 4a.

Here, triphenyl sulfonium triflate (TPS-Tf) was used as the PAG, which generates triflic acid upon UV exposure. A UV lamp with a wavelength of 254 nm and intensity of 14.5 MW/cm^2 was used in this study. Exposure times were typically 60 s, which yields a dose of 870 MJ/cm^2 that is more than sufficient for acid generation from TPS-Tf. For PEO-*b*-PtBA (13.9K, 64 wt % PtBA, PDI = 1.12) blended with 25 wt % L-tartaric acid and 5 wt % TPS-Tf, both the bulk sample and thin film show an order−disorder transition after acid catalyzed deprotection of PtBA during PEB. SAXS (Figure 4b) of the bulk PEO-*b*-PtBA/tartaric acid/TPS-Tf sample after thermal annealing at 90 °C was shown. After UV exposure for 60 s, followed by a thermal bake at 90 °C overnight under vacuum, the system becomes completely disordered, as shown by SAXS (Figure 4c). A similar phenomenon was also observed for a 50 nm thin film, which was spin-coated from a DMF solution. Clear evidence of a well ordered film was observed in atomic force microscopy (AFM) images (Figure 4d) after thermal annealing at 90 °C. The microphase segregated morphology was also confirmed by grazing incidence small-angle X-ray scattering (GISAXS), as shown in Figure 4d. Disorder in the thin film was induced by UV exposure for 60 s and 90 °C baking overnight under vacuum as evidenced by AFM and GISAXS analysis. (Figure 4e). We note here that an annealing step is necessary to allow the system to reach a well-ordered state. For polymers with low molecular weight, the annealing step requires a shorter time. As shown in the Supporting Information (Figure S3), for lower molecular weight PEO-*b*-PtBA (5.2K, 61.7 wt % PtBA, PDI = 1.14), 25 min at 100 °C was sufficient

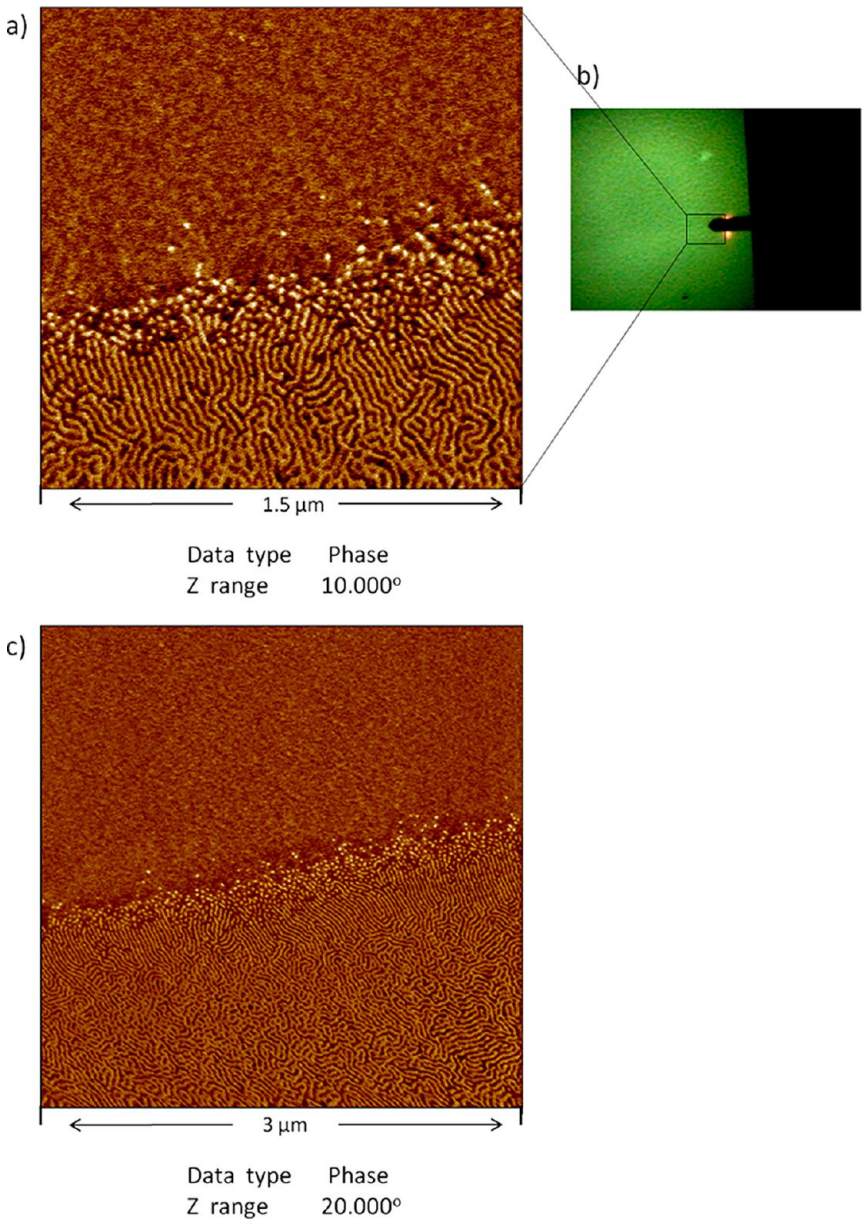

Figure 8. AFM characterization of the film from Figure 7 at the sharp edge of order−disorder pattern: (a) phase image at the scale of 1.5 μm × 1.5 μm; (b) optical microscope attached to the AFM instrument showed the sharp edge of order−disorder pattern during AFM scanning; (c) phase image at the scale of 3 μm × 3 μm.

to achieve a well ordered film. The higher molecular weight sample required several hours.

To achieve sharp order/disorder submicrometer patterns, acid diffusion needs to be minimized during PEB. Image blur during PEB in a patterned, chemically amplified photoresist has been attributed to reaction-diffusion kinetics during PEB.[67,68] Minimizing the time used for the PEB favors high resolution patterning. We used a kinetics study for the disordering transition to optimize the process. Specifically, GISAXS was used to track the disordering transition during the PEB. Three different TPS-Tf loadings in the PEO-*b*-PtBA (18K, 72.3 wt % PtBA, PDI = 1.12)/L-tartaric acid (22 wt %) blend system were characterized in this study: 3 wt %, 7.5 wt %, and 10 wt %. Figure 5 shows that after UV exposure, a 40−60 min PEB was required at 110 °C to disorder the system with the addition of 3 wt % TPS-Tf. The same system required ~15 s with 7.5 wt % TPS-Tf, and only ~6 s with 10 wt % TPS-Tf. Thus, 10 wt % TPS-Tf blends were selected to study the temperature dependence of the disorder transition during PEB. Three different PEB temperatures were used: 110, 100, and 90 °C. As shown in the Supporting Information (Figure S4), the disordering transition was complete during PEB after 6 s at 110 °C as compared to 15 and 22 s at 100 and 90 °C, respectively. Fourier transform infrared spectroscopy (FT-IR) was used to characterize the extent of deprotection of PtBA to yield PAA. Figure S5 in Supporting Information shows the complete deprotection of PtBA using 10 wt % TPS-Tf after UV

flood exposure for 60 s and PEB at 110 °C for 5 and 10 s. FT-IR analysis also indicates hydrogen bond formation between PAA and PEO as shown in the figure.

We next investigated area selective patterning *via* illumination through a mask. To improve pattern resolution, a base quencher can be employed.[69,70] Triethanol amine (0.5 wt %) was loaded into this system to neutralize the trace amounts of acid that may diffuse into the unexposed area. Using DMF as the solvent, PEO-*b*-PtBA (18K, 72.3 wt % PtBA, PDI = 1.12), 22 wt % L-tartaric acid, and 10 wt % TPS-Tf was spin-coated onto a clean silicon wafer to form a 50 nm thick film. After thermal annealing at 90 °C overnight, nicely ordered structures were generated, as characterized by AFM (Figure 6a). GISAXS was used to confirm the ordering (Figure 6b) and showed a lamellar morphology through the integration in the q_// direction (Figure 6c). A photomask was then applied by vacuum to make good contact with the ordered film. After UV exposure for 60 s and a PEB at 110 °C for 10 s, the area exposed to UV became completely disordered, while the area blocked by the mask still kept the ordered structure, as shown by AFM characterization in Figure 7b,d. GISAXS was again used to confirm the structures through the area-selective UV exposure and a PEB. An ordered PEO-*b*-PtBA/L-tartaric acid film with 10 wt % TPS-Tf became completely disordered after a 60 s UV exposure and a 10 s PEB at 110 °C, as observed in the GISAXS spectrum (Figure 7c). The ordered film maintained the ordering after a 10 s baking at 110 °C without UV exposure, as shown by GISAXS measurement (Figure 7e), which rules out the possibility that polymer decomposition during baking causes the disordering. Finally, we used AFM to characterize the order−disorder edge to show the sharp submicrometer patterns of ordered and disordered regions. Figure 8 shows that a very clear pattern of the regions can be observed in a 1.5 μm by 1.5 μm AFM phase image (Figure 8a), and also in a 3 μm by 3 μm AFM phase image (Figure 8c), with the optical microscopy image showing the scanning tip on the order−disorder boundary (Figure 8b). (Height images are shown in the Supporting Information (Figure S6) for reference.) The images suggest weak orientation of the lamellar structures near the edge of the patterns. While we did not investigate this observation further, domain orientation can often be induced by external or non-uniform fields, in this case a chemical potential gradient. There are also indications of spherical domains near the line edge in Figure 8. Spherical domains could emerge as a result of volume reduction of the PtBA-rich domain upon partial deprotection of PtBA, leading to an order−order transition. In any case, these images confirm that the combination of short PEB time and relatively high TPS-Tf loadings and the addition of a trace-amount of amine inhibits acid diffusion and achieves sharp order−disorder patterns on a submicrometer scale even when using a contact mask.

CONCLUSION

We demonstrate a method to achieve submicrometer patterns of well-ordered, microphase separated, and fully disordered regions *via* photoinduced disorder in a block copolymer/additive film. In our example, chemically amplified deprotection of the tBA block in PEO-*b*-PtBA blended with tartaric acid to yield a PAA block induces compatibility of the components, resulting in phase mixing. In this system, the tartaric acid additive plays two important roles. First, it increases segregation strength in PEO-*b*-PtBA, enabling well-ordered systems at low BCP molecular weights. Low molecular weights in turn provide access to small domain spacings and relatively rapid order and disorder kinetics. Second, the presence of tartaric acid suppresses PEO crystallization, resulting in smooth films and eliminating the influence of PEO crystallization on the BCP morphology. The observation that both D- and L-tartaric acid enantiomers are effective additives for these purposes alone, but not in combination where the interaction among the complementary enantiomers is strong relative to the interactions with the polymer segments, illustrates the importance of the additive-chain interactions in driving phase segregation strength.

We point out that the additive strategy in these systems has additional advantages not explored here. For example, one could choose an additive that exhibits strong etch resistance. Using the system design described here, the additive would be confined to the PEO-rich domains in the ordered BCP leaving the PtBA domains unmodified. By comparison the additive is uniformly distributed in the disordered phase. This may in turn enable selective etching of the PtBA domains in the ordered regions relative to both the PEO rich domains in the ordered regions and the phase mixed disordered regions, which also contain the additive. Because there are few constraints on additive selection beyond strong interaction with PEO and PAA generated upon deprotection of the PtBA block, many other designs for the additive for a myriad of applications are possible.

METHODS

Materials. Poly(ethylene glycol) methylether (5K, PDI = 1.06 and 2K, PDI = 1.08) was purchased from Polymer Source. *tert*-Butyl acrylate, anisole, copper(I) bromide(CuBr), copper(II) bromide, and *N*,*N*,*N*′,*N*′,*N*″-pentamethyldiethylenetriamine (PMDETA) were purchased from Acros Organics. Triphenylsulfonium triflate (TPS-Tf) and 2-bromo-2-methylpropionyl bromide were purchased from Sigma-Aldrich.

Block Copolymer Synthesis. A magnetic stir-bar and poly(ethylene glycol) methylether were added to a flame-dried flask capped with a rubber septum, which was evacuated and purged.

Distilled dichloromethane and 2-bromo-2-methylpropionyl bromide (2 molar equiv relative to the PEG polymer) were injected into the flask. Distilled triethylamine was injected dropwise into the flask, which was then stirred at room temperature for 48 h. The reactant was diluted with dichloromethane, extracted by water, and dried with magnesium sulfate. After being precipitated into an excess amount of cold ethanol, the white powder was filtered and dried in a vacuum oven overnight. The product was used as the macroinitiator for chain extension.

Atom transfer radical polymerization (ATRP) was used in chain extension for the synthesis of poly(ethylene oxide-*b*-*tert*-butyl acrylate) (PEO-*b*-PtBA) diblock copolymer following established procedures, with slight modifications.[71] CuBr, the macroinitiator (PEO), and a magnetic stir-bar were added into a Schlenk flask which was capped with a rubber septum and purged with N_2. Anisole and distilled *tert*-butyl acrylate, purged with N_2, were then injected into the flask. When all solids were completely dissolved, three freeze/pump/thaw cycles were applied. After PMDETA was injected into the flask, the final solution was heated at 60 °C for 30 h. Tetrahydrofuran (THF) was used to dilute the reactant, and a column of neutral alumina was used to filter the resulting dark green solution. The final solution was then concentrated through a rotary evaporator and dried in vacuum oven at 70 °C for 24 h.

Polymer Characterization. Gel permeation chromatography (GPC) and ^{1}H NMR spectra were used to characterize the synthesized polymers. GPC was performed in THF at a flow rate of 1.0 mL/min with a column bank consisting of two Polymer Laboratories PLGel Mixed D columns at 40 °C and two detectors, a K-2301 refractive index detector and a K-2600 UV detector. A Bruker DPX300 NMR spectrometer (300 MHz) was used for acquiring ^{1}H NMR spectra using deuterated chloroform as solvent. A Spectrum 100 FT-IR spectrometer (Perkin-Elmer, Inc.) was used for acquiring Fourier transform infrared spectroscopy of PEO-*b*-PtBA films blended with 10 wt % TPS-Tf to measure the extent of PtBA deprotection during PEB and to detect hydrogen bonding between PEO and PAA.

Preparation of Bulk Samples for Small-Angle X-ray Scattering and Wide-Angle X-ray Scattering. PEO-*b*-PtBA and tartaric acid were blended at a given mass ratio in anhydrous ethanol with or without TPS-Tf of a certain weight percentage. Bulk samples were drop cast from the solution onto glass slides while baking at 60 °C and were annealed for 36 h at 90 °C under vacuum.

Small-Angle X-ray Scattering (SAXS) and Wide-Angle X-ray Scattering (WAXS). Dried bulk samples were scraped off the glass slides and placed evenly in the center of metal washers, which were then sandwiched by Kapton film on both sides and placed on a heated vertical holder. For SAXS, the samples were equilibrated at 90 °C for about 20 min and interrogated at 90 °C, while for WAXS, the samples were measured at room temperature. The whole system was evacuated during measurement. WAXS and SAXS in Figures 2 and 3b were done at UMass Amherst using an in-house setup from Molecular Metrology, Inc. (presently sold as Rigaku S-Max3000). A microsource (Bede) of 30 W with a 30 × 30 μm^2 spot size to match a Maxflux optical system (Osmic) gave a low-divergence beam of monochromatic CuKα radiation (wavelength λ = 0.1542 nm). An image plate placed in the sample chamber about 139 mm away from the sample was used to collect WAXS data. Silver behenate was used to calibrate the sample detector distance for SAXS. SAXS measurements in Figure 3a and Figure 4b,c were done at the G1 station of the Cornell High Energy Synchrotron Source (CHESS) with wavelength of X-rays of 0.1453 nm and sample to detector distance of 913 mm using a two-dimensional charge-coupled device (CCD) camera with an image size of 1024 pixels by 1024 pixels.

Differential scanning calorimetry (DSC) characterization was performed using the same bulk samples prepared for SAXS on glass slides. Aluminum pans were filled with 5−10 mg samples and hermetically sealed. The DSC was performed on a TA Instruments Q100 DSC equipped with an RCS cooling system in nitrogen, with a gas flow rate of 50 mL/min. All measurements were done with the heating and cooling rate of 10 °C/min in the temperature range of −90 to 110 °C. The second heating cycle from −80 to 90 °C was reported in this paper. All DSC data were analyzed by using Universal Analysis software from TA Instruments.

Formation of the Ordered Film. Films of about 100 nm thickness were spin-coated from a 3 wt % solution of PEO-*b*-PtBA and L-tartaric acid at a given mass ratio prepared in ethanol with given amount of TPS-Tf onto silicon wafers at 3000 rpm for 20 s for the kinetics study. Films of about 50 nm thickness were spin-coated from a 3 wt % solution of PEO-*b*-PtBA and L-tartaric acid prepared in DMF with TPS-Tf and a trace amount of triethanol amine for the area-selective UV exposure. The films were annealed for 24 h at 90 °C under vacuum.

Grazing Incidence Small-Angle X-ray Scattering (GISAXS) Using Synchrotron Source. All GISAXS measurements were performed at the G1 station of the Cornell High Energy Synchrotron Source (CHESS). The wavelength of X-rays used was 1.2500 Å. The incidence angle was chosen to be above the critical angle of the film under study. The sample to detector distance was 992.3 mm. The scattered radiation was collected with a two-dimensional charge-coupled device (CCD) camera with an image size of 1024 pixels by 1024 pixels.

Atomic Force Microscopy (AFM) Characterization. A Digital Instruments Dimension 3000 scanning microscope in tapping mode was used in AFM topographic and phase images acquisition. The ordered organic films were vacuum-pressed with a photomask and were subject to UV flood exposure for 60 s using a UV lamp with a wavelength of 254 nm and intensity of 14.5 MW/cm^2 to give the dose of 870 MJ/cm^2. A postexposure bake (PEB) was then used to achieve area-selective deprotection of PtBA and to induce the disordering transition. AFM was then used for characterizing the order, disorder, and order/disorder boundary. An optical microscope attached to the AFM was used to monitor the position of the AFM tip on organic films. The thickness of the films was measured using a profilometer (Dektak3) and a Filmetrics Optical Profilometer.

Conflict of Interest: The authors declare no competing financial interest.

Acknowledgment. This work was supported by the NSF Center for Hierarchical Manufacturing (CMMI-1025020). Facilities supported by the Cornell High Energy Synchrotron Source (CHESS) G1 station and the Materials Research Science and Engineering Center at University of Massachusetts Amherst were used in this work with the assistance from Dr. A. Woll, Dr. D. Thirunavukkarasu, and J. Nicholson. We thank M. Beaulieu, Dr. V. Daga, T. Tsai, Dr. Y. Lin, and N. Colella for helpful discussions.

Supporting Information Available: WAXS characterization of racemic tartaric acid and L-tartaric acid; DSC characterization of PEO-*b*-PtBA (9.2K, 46.6 wt % PtBA, PDI = 1.04) blended with 40 wt % L-tartaric acid and 40 wt % D-tartaric acid by heating from −90 to 110 °C with rate of 10 °C/min in an expanded scale; evolution of phase segregation in a thin film of PEO-*b*-PtBA-(5.2K, 61.7 wt % PtBA, PDI = 1.14) with 30% L-tartaric acid during annealing at 100 °C as characterized by GISAXS; kinetic study of the disordering transition during PEB using GISAXS after UV (254 nm) exposure; FT-IR spectra showing the extent of deprotection of *tert*-butyl acrylate in PEO-*b*-PtBA (18K, 72.3 wt % PtBA, PDI = 1.12) film blended with 10 wt % TPS-Tf; AFM characterization of the film shown in Figure 7 at the sharp edge of order−disorder pattern with height images. This material is available free of charge *via* the Internet at http://pubs.acs.org.

REFERENCES AND NOTES

1. Lopes, W. A.; Jaeger, H. M. Hierarchical Self-Assembly of Metal Nanostructures on Diblock Copolymer Scaffolds. *Nature* **2001**, *414*, 735–738.
2. Thurn-Albrecht, T.; Schotter, J.; Kästle, G. A.; Emley, N.; Shibauchi, T.; Krusin-Elbaum, L.; Guarini, K.; Black, C. T.; Tuominen, M. T.; Russell, T. P. Ultrahigh-Density Nanowire Arrays Grown in Self-Assembled Diblock Copolymer Templates. *Science* **2000**, *290*, 2126–2129.
3. Hamley, I. W. Nanotechnology with Soft Materials. *Angew. Chem., Int. Ed.* **2003**, *42*, 1692–1712.

4. Lazzari, M.; López-Quintela, M. A. Block Copolymers as a Tool for Nanomaterial Fabrication. *Adv. Mater.* **2003**, *15*, 1583–1594.
5. Hawker, C. J.; Russell, T. P. Block Copolymer Lithography: Merging "Bottom-Up" with "Top-Down" Processes. *MRS Bull.* **2005**, *30*, 952–966.
6. Park, M.; Harrison, C.; Chaikin, P. M.; Register, R. A.; Adamson, D. H. Block Copolymer Lithography: Periodic Arrays of $\sim 10^{11}$ Holes in 1 Square Centimeter. *Science* **1997**, *276*, 1401–1404.
7. Cheng, J. Y.; Ross, C. A.; Smith, H. I.; Thomas, E. L. Templated Self-Assembly of Block Copolymers: Top-Down Helps Bottom-Up. *Adv. Mater.* **2006**, *18*, 2505–2521.
8. Stoykovich, M. P.; Nealey, P. F. Block Copolymers and Conventional Lithography. *Mater. Today* **2006**, *9*, 20–29.
9. Bates, F. S. Polymer–Polymer Phase Behavior. *Science* **1991**, *251*, 898–905.
10. Niu, S.; Saraf, R. F. Stability of Order in Solvent-Annealed Block Copolymer Thin Films. *Macromolecules* **2003**, *36*, 2428–2440.
11. Kim, S. H.; Misner, M. J.; Xu, T.; Kimura, M.; Russell, T. P. Highly Oriented and Ordered Arrays from Block Copolymers *via* Solvent Evaporation. *Adv. Mater.* **2004**, *16*, 226–231.
12. Kim, S.; Briber, R. M.; Karim, A.; Jones, R. L.; Kim, H. C. Environment-Controlled Spin Coating To Rapidly Orient Microdomains in Thin Block Copolymer Films. *Macromolecules* **2007**, *40*, 4102–4105.
13. Bang, J.; Kim, B. J.; Stein, G. E.; Russell, T. P.; Li, X.; Wang, J.; Kramer, E. J.; Hawker, C. J. Effect of Humidity on the Ordering of PEO-Based Copolymer Thin Films. *Macromolecules* **2007**, *40*, 7019–7025.
14. van Zoelen, W.; Asumaa, T.; Ruokolainen, J.; Ikkala, O.; ten Brinke, G. Phase Behavior of Solvent Vapor Annealed Thin Films of PS-*b*-P4VP(PDP) Supramolecules. *Macromolecules* **2008**, *41*, 3199–3208.
15. Phillip, W. A.; Hillmyer, M. A.; Cussler, E. L. Cylinder Orientation Mechanism in Block Copolymer Thin Films Upon Solvent Evaporation. *Macromolecules* **2010**, *43*, 7763–7770.
16. Albert, J. N. L.; Bogart, T. D.; Lewis, R. L.; Beers, K. L.; Fasolka, M. J.; Hutchison, J. B.; Vogt, B. D.; Epps, T. H. Gradient Solvent Vapor Annealing of Block Copolymer Thin Films Using a Microfluidic Mixing Device. *Nano Lett.* **2011**, *11*, 1351–1357.
17. Morkved, T. L.; Lu, M.; Urbas, A. M.; Ehrichs, E. E.; Jaeger, H. M.; Mansky, P.; Russell, T. P. Local Control of Microdomain Orientation in Diblock Copolymer Thin Films with Electric Fields. *Science* **1996**, *273*, 931–933.
18. Ashok, B.; Muthukumar, M.; Russell, T. P. Confined Thin Film Diblock Copolymer in the Presence of an Electric Field. *J. Chem. Phys.* **2001**, *115*, 1559–1564.
19. Xu, T.; Zhu, Y.; Gido, S. P.; Russell, T. P. Electric Field Alignment of Symmetric Diblock Copolymer Thin Films. *Macromolecules* **2004**, *37*, 2625–2629.
20. Lyakhova, K. S.; Zvelindovsky, A. V.; Sevink, G. J. A. Kinetic Pathways of Order-to-Order Phase Transitions in Block Copolymer Films under an Electric Field. *Macromolecules* **2006**, *39*, 3024–3037.
21. Kim, H.-C.; Park, S.-M.; Hinsberg, W. D. Block Copolymer Based Nanostructures: Materials, Processes, and Applications to Electronics. *Chem. Rev.* **2009**, *110*, 146–177.
22. Hong, S. W.; Huh, J.; Gu, X.; Lee, D. H.; Jo, W. H.; Park, S.; Xu, T.; Russell, T. P. Unidirectionally Aligned Line Patterns Driven by Entropic Effects on Faceted Surfaces. *Proc. Natl. Acad. Sci. U.S.A.* **2012**, *109*, 1402–1406.
23. Park, S.; Lee, D. H.; Xu, J.; Kim, B.; Hong, S. W.; Jeong, U.; Xu, T.; Russell, T. P. Macroscopic 10-Terabit-per-Square-Inch Arrays from Block Copolymers with Lateral Order. *Science* **2009**, *323*, 1030–1033.
24. Cheng, J. Y.; Mayes, A. M.; Ross, C. A. Nanostructure Engineering by Templated Self-Assembly of Block Copolymers. *Nat. Mater.* **2004**, *3*, 823–828.
25. Sundrani, D.; Darling, S. B.; Sibener, S. J. Guiding Polymers to Perfection: Macroscopic Alignment of Nanoscale Domains. *Nano Lett.* **2003**, *4*, 273–276.
26. Sundrani, D.; Darling, S. B.; Sibener, S. J. Hierarchical Assembly and Compliance of Aligned Nanoscale Polymer Cylinders in Confinement. *Langmuir* **2004**, *20*, 5091–5099.
27. Sundrani, D.; Sibener, S. J. Spontaneous Spatial Alignment of Polymer Cylindrical Nanodomains on Silicon Nitride Gratings. *Macromolecules* **2002**, *35*, 8531–8539.
28. Park, S. M.; Stoykovich, M. P.; Ruiz, R.; Zhang, Y.; Black, C. T.; Nealey, P. F. Directed Assembly of Lamellae-Forming Block Copolymers by Using Chemically and Topographically Patterned Substrates. *Adv. Mater.* **2007**, *19*, 607–611.
29. Ruiz, R.; Ruiz, N.; Zhang, Y.; Sandstrom, R. L.; Black, C. T. Local Defectivity Control of 2D Self-Assembled Block Copolymer Patterns. *Adv. Mater.* **2007**, *19*, 2157–2162.
30. Son, J. G.; Hannon, A. F.; Gotrik, K. W.; Alexander-Katz, A.; Ross, C. A. Hierarchical Nanostructures by Sequential Self-Assembly of Styrene-Dimethylsiloxane Block Copolymers of Different Periods. *Adv. Mater.* **2011**, *23*, 634–639.
31. Xu, J.; Russell, T. P.; Ocko, B. M.; Checco, A. Block Copolymer Self-Assembly in Chemically Patterned Squares. *Soft Matter* **2011**, *7*, 3915–3919.
32. Russell, T. P.; Coulon, G.; Deline, V. R.; Miller, D. C. Characteristics of the Surface-Induced Orientation for Symmetric Diblock PS/PMMA Copolymers. *Macromolecules* **1989**, *22*, 4600–4606.
33. Green, P. F.; Christensen, T. M.; Russell, T. P. Ordering at Diblock Copolymer Surfaces. *Macromolecules* **1991**, *24*, 252–255.
34. Smith, A. P.; Sehgal, A.; Douglas, J. F.; Karim, A.; Amis, E. J. Combinatorial Mapping of Surface Energy Effects on Diblock Copolymer Thin Film Ordering. *Macromol. Rapid Commun.* **2003**, *24*, 131–135.
35. Han, E.; Stuen, K. O.; Leolukman, M.; Liu, C.-C.; Nealey, P. F.; Gopalan, P. Perpendicular Orientation of Domains in Cylinder-Forming Block Copolymer Thick Films by Controlled Interfacial Interactions. *Macromolecules* **2009**, *42*, 4896–4901.
36. Choi, S.; Kim, E.; Ahn, H.; Naidu, S.; Lee, Y.; Ryu, D. Y.; Hawker, C. J.; Russell, T. P. Lamellar Microdomain Orientation and Phase Transition of Polystyrene-*b*-poly(methyl methacrylate) Films by Controlled Interfacial Interactions. *Soft Matter.* **2012**, *8*, 3463–3469.
37. Tirumala, V. R.; Daga, V.; Bosse, A. W.; Romang, A.; Ilavsky, J.; Lin, E. K.; Watkins, J. J. Well-Ordered Polymer Melts with 5 nm Lamellar Domains from Blends of a Disordered Block Copolymer and a Selectively Associating Homopolymer of Low or High Molar Mass. *Macromolecules* **2008**, *41*, 7978–7985.
38. Tirumala, V. R.; Romang, A.; Agarwal, S.; Lin, E. K.; Watkins, J. J. Well Ordered Polymer Melts from Blends of Disordered Triblock Copolymer Surfactants and Functional Homopolymers. *Adv. Mater.* **2008**, *20*, 1603–1608.
39. Daga, V. K.; Watkins, J. J. Hydrogen-Bond-Mediated Phase Behavior of Complexes of Small Molecule Additives with Poly(ethylene oxide-*b*-propylene oxide-*b*-ethylene oxide) Triblock Copolymer Surfactants. *Macromolecules* **2010**, *43*, 9990–9997.
40. Daga, V. K.; Anderson, E. R.; Gido, S. P.; Watkins, J. J. Hydrogen Bond Assisted Assembly of Well-Ordered Polyhedral Oligomeric Silsesquioxane-Block Copolymer Composites. *Macromolecules* **2011**, *44*, 6793–6799.
41. Lin, Y.; Daga, V. K.; Anderson, E. R.; Gido, S. P.; Watkins, J. J. Nanoparticle-Driven Assembly of Block Copolymers: A Simple Route to Ordered Hybrid Materials. *J. Am. Chem. Soc.* **2011**, *133*, 6513–6516.
42. Barber, R. P., Jr; Gomez, R. D.; Herman, W. N.; Romero, D. B. Organic Photovoltaic Devices Based on a Block Copolymer/Fullerene Blend. *Org. Electron.* **2006**, *7*, 508–513.
43. Barrau, S.; Heiser, T.; Richard, F.; Brochon, C.; Ngov, C.; van de Wetering, K.; Hadziioannou, G.; Anokhin, D. V.; Ivanov, D. A. Self-Assembling of Novel Fullerene-Grafted Donor–Acceptor Rod–Coil Block Copolymers. *Macromolecules* **2008**, *41*, 2701–2710.
44. Yang, C.; Lee, J. K.; Heeger, A. J.; Wudl, F. Well-Defined Donor–Acceptor Rod–Coil Diblock Copolymers Based on P3HT Containing C60: The Morphology and Role as a

Surfactant in Bulk-Heterojunction Solar Cells. *J. Mater. Chem.* **2009**, *19*, 5416–5423.
45. Urbas, A.; Sharp, R.; Fink, Y.; Thomas, E. L.; Xenidou, M.; Fetters, L. J. Tunable Block Copolymer/Homopolymer Photonic Crystals. *Adv. Mater.* **2000**, *12*, 812–814.
46. Urbas, A.; Fink, Y.; Thomas, E. L. One-Dimensionally Periodic Dielectric Reflectors from Self-Assembled Block Copolymer-Homopolymer Blends. *Macromolecules* **1999**, *32*, 4748–4750.
47. Morikawa, Y.; Kondo, T.; Nagano, S.; Seki, T. Photoinduced 3D Ordering and Patterning of Microphase-Separated Nanostructure in Polystyrene-Based Block Copolymer. *Chem. Mater.* **2007**, *19*, 1540–1542.
48. Chen, W.; Wang, J.-Y.; Zhao, W.; Li, L.; Wei, X.; Balazs, A. C.; Matyjaszewski, K.; Russell, T. P. Photocontrol over the Disorder-to-Order Transition in Thin Films of Polystyrene-*block*-poly(methyl methacrylate) Block Copolymers Containing Photodimerizable Anthracene Functionality. *J. Am. Chem. Soc.* **2011**, *133*, 17217–17224.
49. Rosenhauer, R.; Fischer, T.; Stumpe, J.; Giménez, R.; Piñol, M.; Serrano, J. L.; Viñuales, A.; Broer, D. Light-Induced Orientation of Liquid Crystalline Terpolymers Containing Azobenzene and Dye Moieties. *Macromolecules* **2005**, *38*, 2213–2222.
50. Yu, H.; Iyoda, T.; Ikeda, T. Photoinduced Alignment of Nanocylinders by Supramolecular Cooperative Motions. *J. Am. Chem. Soc.* **2006**, *128*, 11010–11011.
51. Morikawa, Y.; Nagano, S.; Watanabe, K.; Kamata, K.; Iyoda, T.; Seki, T. Optical Alignment and Patterning of Nanoscale Microdomains in a Block Copolymer Thin Film. *Adv. Mater.* **2006**, *18*, 883–886.
52. Tran-Cong-Miyata, Q.; Nishigami, S.; Ito, T.; Komatsu, S.; Norisuye, T. Controlling the Morphology of Polymer Blends Using Periodic Irradiation. *Nat. Mater.* **2004**, *3*, 448–451.
53. Inoue, K.; Komatsu, S.; Trinh, X.-A.; Norisuye, T.; Tran-Cong-Miyata, Q. Local Deformation in Photo-Crosslinked Polymer Blends Monitored by Mach-Zehnder Interferometry. *J. Polym. Sci., Part B: Polym. Phys.* **2005**, *43*, 2898–2913.
54. Trinh, X.-A.; Fukuda, J.; Adachi, Y.; Nakanishi, H.; Norisuye, T.; Tran-Cong-Miyata, Q. Effects of Elastic Deformation on Phase Separation of a Polymer Blend Driven by a Reversible Photo-Cross-Linking Reaction. *Macromolecules* **2007**, *40*, 5566–5574.
55. Daga, V. K.; Schwartz, E. L.; Chandler, C. M.; Lee, J.-K.; Lin, Y.; Ober, C. K.; Watkins, J. J. Photoinduced Ordering of Block Copolymers. *Nano Lett.* **2011**, *11*, 1153–1160.
56. Lestel, L.; Guegan, P.; Boileau, S.; Cheradame, H.; Laupretre, F. Influence of the Chemical Nature of Cross-Links on the Local Dynamics of Bulk Poly(ethylene oxide) Networks as Studied by Carbon-13 NMR at Temperatures Well above the Glass-Transition Temperature. *Macromolecules* **1992**, *25*, 6024–8.
57. Cypcar, C. C.; Camelio, P.; Lazzeri, V.; Mathias, L. J.; Waegell, B. Prediction of the Glass Transition Temperature of Multicyclic and Bulky Substituted Acrylate and Methacrylate Polymers Using the Energy, Volume, Mass (EVM) QSPR Model. *Macromolecules* **1996**, *29*, 8954–8959.
58. Ruokolainen, J.; Mäkinen, R.; Torkkeli, M.; Mäkelä, T.; Serimaa, R.; Brinke, G. t.; Ikkala, O. Switching Supramolecular Polymeric Materials with Multiple Length Scales. *Science* **1998**, *280*, 557–560.
59. Ruokolainen, J.; Saariaho, M.; Ikkala, O.; ten Brinke, G.; Thomas, E. L.; Torkkeli, M.; Serimaa, R. Supramolecular Routes to Hierarchical Structures: Comb-Coil Diblock Copolymers Organized with Two Length Scales. *Macromolecules* **1999**, *32*, 1152–1158.
60. Bondzic, S.; de Wit, J.; Polushkin, E.; Schouten, A. J.; ten Brinke, G.; Ruokolainen, J.; Ikkala, O.; Dolbnya, I.; Bras, W. Self-Assembly of Supramolecules Consisting of Octyl Gallate Hydrogen Bonded to Polyisoprene-block-poly(vinylpyridine) Diblock Copolymers. *Macromolecules* **2004**, *37*, 9517–9524.
61. Epps, T. H.; Bailey, T. S.; Waletzko, R.; Bates, F. S. Phase Behavior and Block Sequence Effects in Lithium Perchlorate-Doped Poly(isoprene-*b*-styrene-*b*-ethylene oxide) and Poly(styrene-*b*-isoprene-*b*-ethylene oxide) Triblock Copolymers. *Macromolecules* **2003**, *36*, 2873–2881.
62. Epps, T. H.; Bailey, T. S.; Pham, H. D.; Bates, F. S. Phase Behavior of Lithium Perchlorate-Doped Poly(styrene-*b*-isoprene-*b*-ethylene oxide) Triblock Copolymers. *Chem. Mater.* **2002**, *14*, 1706–1714.
63. Santagata, N. M.; Lakhani, A. M.; Davis, B. F.; Luo, P.; Buongiorno Nardelli, M.; Pearl, T. P. Chiral Steering of Molecular Organization in the Limit of Weak Adsorbate-Substrate Interactions: Enantiopure and Racemic Tartaric Acid Domains on Ag(111). *J. Phys. Chem. C* **2010**, *114*, 8917–8925.
64. Ito, H. Chemical Amplification Resists for Microlithography. *Adv. Polym. Sci.* **2005**, *172*, 37–245.
65. Hinsberg, W.; Houle, F.; Wallraff, G.; Sanchez, M.; Morrison, M.; Hoffnagle, J.; Ito, H.; Nguyen, C.; Larson, C. E.; Brock, P. J.; et al. Factors Controlling Pattern Formation in Chemically Amplified Resists at Sub-100 nm Dimensions. *J. Photopolym. Sci. Technol.* **1999**, *12*, 649–662.
66. Hinsberg, W. D.; Houle, F. A.; Sanchez, M. I.; Wallraff, G. M. Chemical and Physical Aspects of the Post-Exposure Baking Process Used for Positive-Tone Chemically Amplified Resists. *IBM J. Res. Dev.* **2001**, *45*, 667–681.
67. Houle, F. A.; Hinsberg, W. D.; Morrison, M.; Sanchez, M. I.; Wallraff, G.; Larson, C.; Hoffnagle, J. Determination of Coupled Acid Catalysis-Diffusion Processes in a Positive-Tone Chemically Amplified Photoresist. *J. Vac. Sci. Technol., B* **2000**, *18*, 1874–1885.
68. Houle, F. A.; Hinsberg, W. D.; Sanchez, M. I.; Hoffnagle, J. A. Influence of Resist Components on Image Blur in a Patterned Positive-Tone Chemically Amplified Photoresist. *J. Vac. Sci. Technol., B* **2002**, *20*, 924–931.
69. Michaelson, T. B.; Pawloski, A. R.; Acheta, A.; Nishimura, Y.; Willson, C. G. The Effects of Chemical Gradients and Photoresist Composition on Lithographically Generated Line Edge Roughness. *Proc. SPIE* **2005**, 368–379.
70. Houle, F. A.; Hinsberg, W. D.; Sanchez, M. I. Acid-Base Reactions in a Positive Tone Chemically Amplified Photoresist and Their Effect on Imaging. *J. Vac. Sci. Technol., B* **2004**, *22*, 747–757.
71. Davis, K. A.; Charleux, B.; Matyjaszewski, K. Preparation of Block Copolymers of Polystyrene and Poly(*t*-butyl acrylate) of Various Molecular Weights and Architectures by Atom Transfer Radical Polymerization. *J. Polym. Sci. A, Polym. Chem.* **2000**, *38*, 2274–2283.